Liquid surface model for carbon nanotube energetics

Ilia A. Solov'yov,[*,†] Maneesh Mathew, Andrey V. Solov'yov,[†] and Walter Greiner
Frankfurt Institute for Advanced Studies, Goethe University, Ruth-Moufang-Strasse 1, 60438 Frankfurt am Main, Germany
(Received 9 May 2008; revised manuscript received 10 September 2008; published 13 November 2008)

In the present paper we developed a model for calculating the energy of single-wall carbon nanotubes of arbitrary chirality. This model, which we call as the liquid surface model, predicts the energy of a nanotube with relative error less than 1% once its chirality and the total number of atoms are known. The parameters of the liquid surface model and its potential applications are discussed. The model has been suggested for open end and capped nanotubes. The influence of the catalytic nanoparticle, atop which nanotubes grow, on the nanotube stability is also discussed. The suggested model gives an important insight in the energetics and stability of nanotubes of different chirality and might be important for the understanding of nanotube growth process. For the computations we use empirical Brenner and Tersoff potentials and discuss their applicability to the study of carbon nanotubes. From the calculated energies we determine the elastic properties of the single-wall carbon nanotubes (Young modulus, curvature constant) and perform a comparison with available experimental measurements and earlier theoretical predictions.

DOI: 10.1103/PhysRevE.78.051601 PACS number(s): 61.48.De, 61.46.Np, 81.07.De, 62.20.de

I. INTRODUCTION

Right from the initial report of the existence of carbon nanotubes by Iijima [1], studies have been performed to understand their properties. Carbon nanotubes are tube-shaped nanostructures of carbon with electrical, mechanical, and thermal properties that derive from the special features of carbon bonds, their quasi-one-dimensional nature, and their cylindrical symmetry. These properties include very high elastic modulus, tensile strength, thermal conductivity, and electrical conductivity (see, for example, [2–6] and references therein).

Carbon nanotubes have radii typically ranging from 0.2 nm to tens of nanometers [7] and lengths of up to several millimeters [8]. They are considered to be one of the strongest materials discovered so far. The Young's modulus and shear modulus of a typical nanotube are calculated and is found to be comparable to those of diamond [9–11]. Experimental studies have confirmed this [12]. The Young's modulus obtained by different studies lies in the range of 0.32–5.5 TPa [9–23] for a nanotube while for stainless steel it is of the range of 0.1–0.2 TPa [24]. Another important feature of carbon nanotubes is their softness to lateral forces. There are studies using molecular dynamics methods which show that under axial compression, a single-wall nanotube buckles and eventually undergoes shape changes [25]. These shape changes result in an abrupt release of energy and a singularity in the stress-strain curve [26], which can be treated as a structural phase transition in carbon nanotubes [27–29]. Another important property of carbon nanotubes is their high elastic flexibility. Iijima and co-workers observed fully reversible bending of carbon nanotubes by high resolution electron microscopy [30,31].

Chemical vapor deposition (CVD) is a standard technique for obtaining high quality carbon nanotubes in technologically significant quantities [32–34]. In catalytic CVD a patterned array of catalyst nanoparticles (typically, Ni, Co or Fe nanoclusters) is attached to a substrate. It allows one to grow vertically aligned nanotube arrays, very well suited for various applications in thin films development, electronics, biophysics, etc. There are numerous empirical recipes for improving production efficiency and quality of the carbon nanotubes, such as, e.g., plasma-enhanced CVD [35]. However, in spite of intensive research and a huge amount of experimental knowledge, the physical mechanisms leading to the catalytically assisted carbon nanotubes growth remain a widely debated issue. It is evident that a breakthrough in understanding the growth mechanisms would facilitate further improvements in the growing technologies leading to a better quality of the nanotubes and to a better control over the nanotubes properties.

Because of their unique properties, carbon nanotubes have been considered as potential candidates for a variety of electrical, mechanical, and chemical applications. However, in order to use them commercially, many issues need to be resolved. One of the major issues is the controlling of the chirality of carbon nanotubes during its synthesis. Chirality is a special property of nanotube which describes how much it is twisted, and is defined by two integer numbers n and m, which are called chiral indices. Most of the important electrical, mechanical and chemical properties of carbon nanotubes are dependant on the chirality of the nanotube [5,6,9,13,36–38]. Hence, a detailed study on how the chirality of a nanotube influences its energetics is very important for a proper understanding of various properties of nanotubes.

In this paper we propose a model for calculating the energy of single-wall carbon nanotubes of arbitrary chirality. It assumes that the total energy of a single-wall nanotube can be written as a sum of surface, curvature, and edge energy terms. The first model of this kind was proposed by Lord Rayleigh in 1882 in his studies on stability of charged droplets and was called the liquid drop model. Later on, Born and Wheeler developed a similar model to explain the fission of

*ilia@fias.uni-frankfurt.de
†On leave from the A.F. Ioffe Institute, St. Petersburg, Russia

large nuclei [39]. The liquid drop model was also used for the study of atomic clusters [40–44].

Because of the similarity of the suggested model to that used in the study of liquid droplets, nuclei, and clusters we adopted the name liquid surface model. Similar models were already discussed for nanotubes [45–50], but the studies were limited only to specific types of nanotubes, namely zigzag and armchair. Contrary to the earlier studies, our model can be applied to nanotubes of arbitrary chirality and length. The major difference between the liquid drop model and the liquid surface model is that for single-wall nanotubes the liquid surface model does not contain a volume energy part. The volume energy appears in the liquid surface model in the case of multiwall nanotubes.

We have investigated open end carbon nanotubes with chiral index n varying from $n=5$ to $n=10$, while index m varies from $m=0$ to $m=5$. For each chirality, the energy of nanotubes of different lengths was calculated and the dependence of the binding energy on the nanotube length was obtained. The results of the calculations were used to determine the parameters of the liquid surface model.

Open end nanotubes can be produced in experiment [51–53], but are difficult to study, because of the high reactivity of the edge atoms [54]. Thus in many experiments nanotubes form caps of carbon atoms [55,56]. Beside this fact, in the CVD process nanotubes grow from the catalytic metal nanoparticle and the interaction between the catalytic nanoparticle and the nanotube plays an important role on the stability of the system. In the present paper we apply the liquid surface model to the capped nanotubes and study how the catalytic nanoparticle impacts on the energy of the system. We have studied capped nanotubes of the following chiralities: (5,0); (6,0); (5,5); (9,0); (10,0); (6,6); (12,3); (10,10); (15,5); (19,0); (11,11); (23,0); (16,16); (28,0).

Carbon based structures are often modeled with the use of the so-called bond-order potentials [15–17,57], which account for neighbors of each atom. The two widely used bond-order potentials are the Tersoff potential [58] and the Brenner potential [11,59]. It is believed that the Brenner potential accounts more accurately for the π-bondings in the system, and therefore is better for the description of carbon nanotubes [11,59,60]. In this paper we illustrate that both potentials lead to similar results and can be used for modeling of carbon nanotubes.

To stress the differences between the Tersoff and the Brenner potential we described the interaction between atoms in the open end nanotubes using Tersoff potential, while we used Brenner potential for the capped nanotubes. For chiralities (5,5); (5,0); (6,0); and (9,0) we additionally calculated the capped nanotubes using the Tersoff potential and performed a comparison of energies obtained with the use of both potentials. We also calculated the curvature energy for nanotubes of different radii and from this dependence determined the curvature constant and the Young modulus for the single-wall carbon nanotubes. The calculated values were compared with results of available experimental measurements and earlier theoretical calculations.

II. THEORETICAL METHODS

For the sake of completeness, we introduce the idea of chirality of nanotubes in Sec. II A. Section II B is devoted to the discussion of the Tersoff and Brenner potentials, which were used for the description of nanotubes. Sections II C and II D describe the liquid surface model and its parameters in the case of the open end and capped nanotubes respectively.

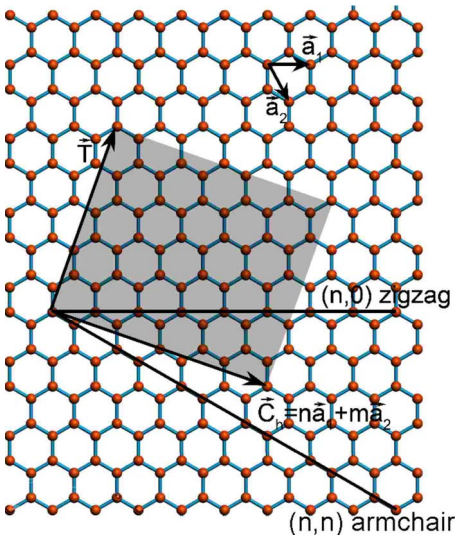

FIG. 1. (Color online) Construction of a nanotube from a graphene sheet. The vectors $\vec{a}_1$, $\vec{a}_2$ are the basis vectors in the graphene sheet. The chiral index n is the number of steps in the $\vec{a}_1$ direction and the chiral index m is that in the $\vec{a}_2$ direction. $\vec{C}_h=n\vec{a}_1+m\vec{a}_2$ is the chirality vector, and $\vec{T}$ is the translation vector and is in the direction of the tube axis. The chiral vector directions for both zigzag ($m=0$) and armchair ($m=n$) nanotubes are indicated.

A. Nanotube chirality

Carbon nanotubes are modeled as cylinders of carbon atoms rolled from a graphene sheet. The idea of obtaining a carbon nanotube from a graphene sheet as well as the concepts of zigzag, armchair, and chiral nanotubes are illustrated in Fig. 1. The way of rolling the graphene sheet determines the chirality of a nanotube [7,61]. The chirality is specified by two integer numbers, n and m, where $0 \leqslant m \leqslant n$. If $m=0$, the nanotube is called zigzag while if $m=n$, it is called armchair. All other nanotubes are called chiral nanotubes [61]. The vector in the graphene sheet, defined by n and m is called the chirality vector. In Fig. 1 it is denoted as $\vec{C}_h$. To define the chirality vector, two basis vectors $\vec{a}_1$ and $\vec{a}_2$ are introduced. The chiral indices n and m are the number of steps that should be taken along the $\vec{a}_1$ and $\vec{a}_2$ directions, respectively, in order to reach the tip of the chirality vector. To construct the nanotube, the graphene sheet is folded along the chirality vector. The vector along the axial direction of the nanotube is called the translation vector. It is perpendicular to the chirality vector and in Fig. 1, it is denoted as $\vec{T}$.

B. Energy calculation

To study the structure and energetics of carbon nanotubes, we used the bond-order Tersoff [58] and Brenner [59]

empirical potentials, which were developed for covalent systems and parametrized for carbon [59,62]. Both potentials are many-body potentials, which depend on the nearest neighbors of atoms and have the following form:

$$V_{ij} = f_C(r_{ij})[f_R(r_{ij}) - b_{ij} f_A(r_{ij})]. \tag{1}$$

Here, $f_C(r_{ij})$ is the cutoff function which limits the interaction of an atom to its nearest neighbors, which is defined as

$$f_C(r_{ij}) = \begin{cases} 1, & r_{ij} \leqslant R - D, \\ \frac{1}{2} - \frac{1}{2}\sin\left(\frac{\pi}{2}(r_{ij} - R)/D\right), & R - D < r_{ij} \leqslant R + D, \\ 0, & r_{ij} > R + D, \end{cases} \tag{2}$$

where r_{ij} is the distance between the ith and the jth atoms, R and D are parameters which determine the range of the potential and are taken from Ref. [62] for the Tersoff potential and from Refs. [11,59] for the Brenner potential. The functions $f_R(r_{ij})$ and $f_A(r_{ij})$ in Eq. (1) are the repulsive and the attractive terms of the potential, respectively. In the case of the Tersoff potential these terms are defined as follows:

$$f_R(r_{ij}) = A \exp(-\lambda_1 r_{ij}), \tag{3}$$

$$f_A(r_{ij}) = B \exp(-\lambda_2 r_{ij}). \tag{4}$$

Here, A, B, λ_1, and λ_2 are positive parameters of the potential, which were derived for carbon in Ref. [62]. The Brenner potential implies the following parametrization for f_R and f_A:

$$f_R(r_{ij}) = \frac{D_e}{S-1} \exp[-\sqrt{2S}\lambda(r_{ij} - R_e)], \tag{5}$$

$$f_A(r_{ij}) = \frac{D_e S}{S-1} \exp[-\sqrt{2/S}\lambda(r_{ij} - R_e)], \tag{6}$$

where the parameters D_e, S, λ, and R_e are determined from the known physical properties of carbon, graphite, and diamond [11,59]. The factor b_{ij} in Eq. (1) is the so-called bond order term, which is defined as follows:

$$b_{ij} = [1 + (\beta\zeta_{ij})^{n_0}]^{-\delta}, \tag{7}$$

where β and n are parameters of the potential, while ζ_{ij} is defined as:

$$\zeta_{ij} = \sum_{k \neq i,j} f_C(r_{ik}) g(\theta_{ijk}). \tag{8}$$

Here, $f_C(r_{ik})$ is the cutoff function introduced in Eq. (2). The function $g(\theta_{ijk})$ is defined as

$$g(\theta_{ijk}) = a\left(1 + \frac{c^2}{d^2} - \frac{c^2}{d^2 + (h - \cos\theta_{ijk})^2}\right), \tag{9}$$

where θ_{ijk} is the angle between bonds formed by pairs of atoms (i,j) and (i,k).

The Tersoff and Brenner potentials were used earlier for the studies of stability and for the calculation of the structural properties of many carbon systems including fullerenes [60,63–65] and nanotubes [11,48,50,66]. The parameters of both potentials are slightly different in different papers. In Table I, we compile the parameters used in the present paper which are consistent with those discussed in Refs. [11,59,62].

C. Liquid surface model: Open end nanotubes

Let us consider an open end nanotube. According to the liquid surface model, the total energy of a nanotube can be expressed as a sum of three terms which are determined by the nanotube geometry, namely, the surface area, curvature of the surface, and the edge

$$E = E_s + E_c + E_e. \tag{10}$$

In order to understand the origin of these three different energy contributions, consider a graphene sheet shown in Fig. 1. The energy of the plane sheet depends on the total number of atoms in it. For a graphene sheet of finite size, there are two kinds of carbon atoms: Atoms within the sheet and atoms at the edge of the sheet. Hence, the energy of the

TABLE I. Parameters of the Tersoff [62] and Brenner [11,59] potentials used in the calculations.

Tersoff parameter	Tersoff value	Brenner parameter	Brenner value
A (eV)	1393.6	D_e (eV)	6.325
B (eV)	346.74	S	1.29
λ_1 (Å^{-1})	3.4879	λ (Å^{-1})	1.5
λ_2 (Å^{-1})	2.2119	R_e (Å)	1.315
$\beta \times 10^{-7}$	1.5724	β	1.0
n_0	0.7275	n_0	1.0
δ	0.6873	δ	0.80469
a	1	a	0.011304
c	38049	c	19
d	4.3484	d	2.5
h	−0.57058	h	−1.0
R (Å)	1.95	R (Å)	1.85
D (Å)	0.15	D (Å)	0.15

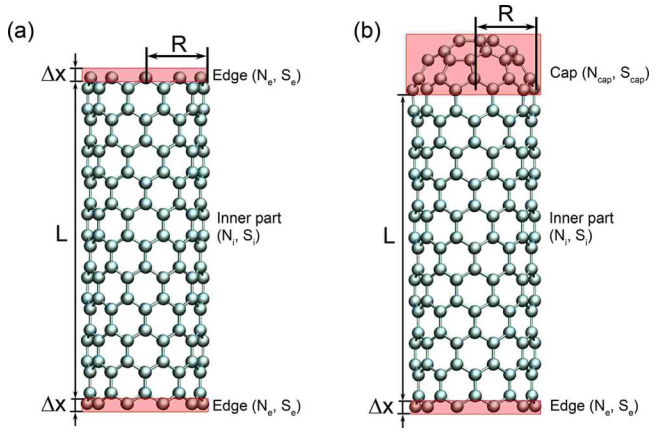

FIG. 2. (Color online) Different parts of the nanotube considered in the liquid surface model are shown. (a) Open end nanotube; (b) capped nanotube. Δx is the width of the edge region of the nanotube, N_e and S_e are the number of atoms in the edge region and the area of this region, respectively. N_i and S_i are the number of atoms in the inner region and its surface area, respectively. L and R are the length and the radius of the nanotube. N_{cap} and S_{cap} are the number of atoms in the cap and its surface area, respectively.

sheet depends on two quantities: Its surface and the number of atoms at the edge. The edge energy arises from the carbon atoms at the edge which have dangling bonds. When the graphene sheet is rolled up to form a nanotube, two edges of the sheet meet each other resulting in closing of dangling bonds along those edges. This leads to a decrease of edge energy in the nanotube compared to that in the graphene sheet. But at the same time, the rolling up of the graphene sheet causes an increase of the strain energy in a nanotube, i.e., elastic energy needed to roll a planar sheet up into a cylinder. The edge energy is directly proportional to the number of dangling bonds at the edge, which in the case of a nanotube is equal to the number of carbon atoms at the edge. For a nanotube of chirality (n,m), the number of carbon atoms at one edge is given by $n+m$.

In order to derive explicit expressions for the energy contributions, we define that a nanotube consists of two parts—the two edges of length Δx, and the inner part of length L [see Fig. 2(a)]. Δx is defined in such a manner that all carbon atoms with less than three bonds are part of it.

If N_i is the number of carbon atoms in the inner part of the nanotube and N_e is that at one edge, the total number of atoms in the nanotube can be written as

$$N = N_i + 2N_e. \tag{11}$$

Let ρ_i be the area per atom in the inner region. Then the surface area of the inner region of the nanotube can be written as

$$S_i = 2\pi RL = \rho_i N_i = \rho_i N - 2\rho_i N_e. \tag{12}$$

Here R is the radius of the nanotube and L is its length, as illustrated in Fig. 2. If σ is energy density per atom and $\sigma_c = \epsilon_c / R^2$ is the curvature energy per atom; ρ_e is the area per atom at the edge of the nanotube, then the surface, edge, and curvature energy terms can be written as follows:

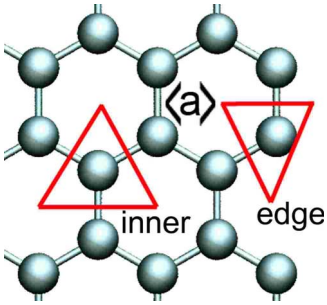

FIG. 3. (Color online) Area per atom in the inner and edge regions of a nanotube. $\langle a \rangle$ indicates the average bond length in a nanotube.

$$E_s = \int_{S_i} \sigma dS = \sigma S_i, \tag{13}$$

$$E_c = \int_{S_i+2S_e} \sigma_c dS = \int_{S_i+2S_e} \epsilon_c \frac{1}{R^2} dS = \epsilon_c \frac{S_i + 2S_e}{R^2}, \tag{14}$$

$$E_e = 2\sigma \Delta x (2\pi R) = 2\sigma \rho_e N_e. \tag{15}$$

Here S_e is the area of the edge of the nanotube and ϵ_c is the specific curvature energy of a nanotube. Substituting Eqs. (13)–(15) into Eq. (10), one derives

$$E = \sigma S_i + \epsilon_c \frac{S_i + 2S_e}{R^2} + 2\sigma \rho_e N_e. \tag{16}$$

Substituting S_i from Eq. (12), one obtains

$$E = \sigma \rho_i (N - 2N_e) + \epsilon_c \frac{\rho_i N - 2\rho_i N_e + 2\rho_e N_e}{R^2} + 2\sigma \rho_e N_e. \tag{17}$$

Rearranging the terms,

$$E = \left(\sigma \rho_i + \frac{\epsilon_c \rho_i}{R^2} \right) N + 2 \left(\sigma \rho_e - \sigma \rho_i - \frac{\epsilon_c \rho_i}{R^2} + \frac{\epsilon_c \rho_e}{R^2} \right) N_e, \tag{18}$$

where $N_e = n+m$. The radius of the nanotube is determined by the chiral indices n and m [5,7],

$$R = \frac{\sqrt{3}\langle a \rangle}{2\pi} \sqrt{n^2 + m^2 + nm}, \tag{19}$$

where $\langle a \rangle$ is the average interatomic distance in the nanotube. The area per atom in the inner region of a nanotube can be calculated as the area of a triangle shown in Fig. 3 and reads as

$$\rho_i = \frac{3\sqrt{3}}{4} \langle a \rangle^2. \tag{20}$$

The area per atom at the edge of a nanotube is smaller and can be written as

$$\rho_e = \alpha\rho_i, \tag{21}$$

where $\alpha \in [0\cdots 1]$ is a dimensionless parameter. Substituting Eqs. (19)–(21) into Eq. (18) and clubbing all constants, one obtains

$$E = \sqrt{3}\left(\frac{3\langle a\rangle^2\sigma}{4} + \frac{\pi^2\epsilon_c}{n^2+m^2+nm}\right)[N + 2(\alpha-1)(n+m)]. \tag{22}$$

As follows from Eq. (22) the energy of a nanotube depends on the energy density per atom σ, the specific curvature energy ϵ_c, and parameter α defining the ratio of the area per edge atom to the area per atom in the inner region of a nanotube. If the total number of atoms and the chirality of the nanotube are known, the total energy and the binding energy per atom can be calculated using Eq. (22). In order to determine the parameters σ, ϵ_c, and α, we consider nanotubes with chiralities ranging from $n=5$ to $n=10$, where for each n, $0 \leqslant m \leqslant 5$ and $N=50-450$. By fitting the numerically calculated values of energy with Eq. (22) one derives the values for the parameters σ, ϵ_c, and α. The results are discussed in Sec. III in detail.

D. Liquid surface model: Capped nanotubes

The liquid surface model can also be applied to the study of capped nanotubes. In this case the total energy of a nanotube reads as

$$E = E_s^{\text{tube}} + E_c^{\text{tube}} + E_s^{\text{cap}} + E_c^{\text{cap}} + E_e, \tag{23}$$

where E_s, E_c and E_e are the energies of the surface, curvature, and the edge, respectively. Superscripts "tube" and "cap" refer to the cylindrical and the cap parts of the nanotube, respectively. The total number of atoms in a capped nanotube can be written as

$$N = N_i + N_e + N_{\text{cap}}, \tag{24}$$

where N_i, N_e, and N_{cap} are the number of carbon atoms in the inner part of the nanotube, at the edge and the number of atoms in the cap [see Fig. 2(b)] which reads as

$$N_{\text{cap}} = \frac{S_{\text{cap}}}{\rho_{\text{cap}}} = \frac{2\pi R^2}{\rho_{\text{cap}}}. \tag{25}$$

Here S_{cap} is the surface area of the cap, and ρ_{cap} is the area per atom in the cap. The surface energy term of a nanotube with a cap can thus be written as

$$E_s^{\text{tube}} = \sigma\rho_i(N - N_{\text{cap}} - N_e) = \sigma\rho_i\left(N - \frac{2\pi R^2}{\rho_{\text{cap}}} - N_e\right). \tag{26}$$

Since a capped nanotube has only one edge the curvature energy term reads as

$$E_c^{\text{tube}} = \int_{S_i+S_e} \epsilon_c \frac{1}{R^2} dS = \frac{\epsilon_c\rho_i}{R^2}N + \frac{\epsilon_c(\rho_e-\rho_i)}{R^2}N_e - \frac{2\pi\epsilon_c\rho_i}{\rho_{\text{cap}}}. \tag{27}$$

The edge energy term in Eq. (23) is defined as

$$E_e = \sigma\Delta x(2\pi R) = \sigma\rho_e N_e. \tag{28}$$

The surface and curvature energies of the cap in Eq. (23) can be written as follows:

$$E_s^{\text{cap}} = \int_{S_{\text{cap}}} \sigma dS = \sigma S_{\text{cap}} = 2\pi\sigma R^2, \tag{29}$$

$$E_c = \int_{S_{\text{cap}}} \epsilon_c^{\text{cap}} \frac{1}{R^2} dS = 2\pi\epsilon_c^{\text{cap}}. \tag{30}$$

Substituting Eqs. (26)–(30) into Eq. (23), one derives

$$E = \left(\sigma\rho_i + \frac{\epsilon_c\rho_i}{R^2}\right)N + \left(\sigma(\rho_e-\rho_i) + \frac{\epsilon_c(\rho_e-\rho_i)}{R^2}\right)N_e + \frac{2\pi\sigma}{\rho_{\text{cap}}}(\rho_{\text{cap}}-\rho_i)R^2 + 2\pi\epsilon_c^{\text{cap}} - \frac{2\pi\epsilon_c\rho_i}{\rho_{\text{cap}}}. \tag{31}$$

The area per atom in the inner part of the nanotube can be related with the area per atom in the cap as follows:

$$\rho_i = \gamma\rho_{\text{cap}}. \tag{32}$$

Substituting Eqs. (19)–(21) and Eq. (32) into Eq. (31) and clubbing all constants, one obtains

$$E = \sqrt{3}\left(\frac{3\langle a\rangle^2\sigma}{4} + \frac{\pi^2\epsilon_c}{n^2+m^2+nm}\right)[N + (\alpha-1)(n+m)] + \frac{3\langle a\rangle^2\sigma}{2\pi}(1-\gamma)(n^2+m^2+nm) + 2\pi(\epsilon_c^{\text{cap}} - \epsilon_c\gamma). \tag{33}$$

The last two terms in Eq. (33) account for the structure of the nanotube cap, while the first term corresponds to the energy of an open end nanotube with one edge (see Sec. II C). Thus the energy of a capped nanotube is determined by the five parameters: Energy density per atom σ, the specific curvature energies ϵ_c and ϵ_c^{cap}, as well as parameters α and $1/\gamma$ defining the ratio of the area per edge atom and the area of an atom in the cap to the area per atom in the inner region of a nanotube.

III. RESULTS AND DISCUSSION

A. Parameters of the liquid surface model

To calculate parameters (σ, ϵ_c, α) for the open end and (σ, ϵ_c, ϵ_{cap}, α, γ) for the capped nanotubes we considered structures of different length and chirality. To determine the parameters of the liquid surface model for the open end nanotubes we have calculated the energies for the structures with $N=50-450$, $n=5-10$, and $m=0-5$ and fitted the obtained values with Eq. (22). The calculation for the capped nanotubes is more difficult, because one needs to construct a cap for a nanotube of a given chirality.

We have used the following procedure for the nanotube cap construction. A nanotube of chirality (n,m) has $n+m$ atoms at the edge which should form bonds with the cap. The cap should be one-half of a fullerene with the radius equal to the radius of the nanotube. The construction of the fullerene

TABLE II. Values for the parameters σ, ϵ_c, ϵ_{cap}, α, and γ used in the liquid surface model for open end and capped nanotubes.

Nanotube type	σ (eV/Å^2)	ϵ_c (eV)	ϵ_{cap} (eV)	α	γ
Open end	−2.8669	0.5879		0.6925	
Capped	−2.8564	0.3550	0.6624	0.6900	0.9998

starts either from a hexagon or a pentagon and is continued by adding hexagons and pentagons sequentially row by row around the initial one. This procedure has been well described, e.g., in Ref. [67]. For the C_{60} family of fullerenes (e.g., C_{60}, C_{240}, C_{720}) only certain radii are possible and therefore only some chiralities can be capped with an ideal semifullerene. To construct a cap for arbitrary chirality one needs to introduce one or several defects (for example, to place a pentagonal ring instead of a hexagonal one) in the cap structure. In the present paper we demonstrate this on several examples.

To calculate parameters of the liquid surface model for capped nanotubes we considered structures with chiralities (5,0); (6,0); (5,5); (9,0); (10,0); (6,6); (12,3); (10,10); (15,5); (19,0); (11,11); (23,0); (16,16); (28,0), containing $N=50-3000$ atoms.

The resulting values of (σ, ϵ_c, α) for the open end and of (σ, ϵ_c, ϵ_{cap}, α, γ) for the capped nanotubes are compiled in Table II. For the calculation of the open end nanotubes we used the Tersoff potential, while the capped nanotubes were studied with the use of the Brenner potential.

Parameters σ, ϵ_c, and α should be the same for the open end and capped nanotubes. From Table II follows that for both cases parameters σ and α are very close to each other, and parameters ϵ_c are of the same order of magnitude. The differences arise because different potentials were used for the computation of parameters for the open end and capped nanotubes.

It is also worth noting that parameter γ is very close to unity, indicating that the area per atom in the inner part of a nanotube is almost the same as the area per atom in the cap as follows from Eq. (32).

B. Analysis of binding energy per atom

As predicted by the liquid surface model the total binding energy for an open end and capped nanotube is given by Eqs. (22) and (33), respectively. The binding energy per atom reads as

$$\epsilon = \frac{E}{N}, \tag{34}$$

where E is the total energy of a nanotube and N is the total number of atoms in it. The result of comparison of the binding energy per atom predicted by the liquid surface model and that calculated using the Tersoff potential for the open end nanotubes is illustrated in Fig. 4, which shows the dependence of the binding energy on the total number of atoms in the system. Different symbols (squares, triangles, stars, dots) in Fig. 4 represent the values calculated using the Tersoff potential and the lines near the corresponding symbols show the predictions of the liquid surface model.

Figure 4 shows that nanotubes become more stable as their length increases. This happens because of the nanotube's edge. If L is the length of a nanotube and R is its radius, one can introduce a parameter to characterize the edge of a nanotube as follows:

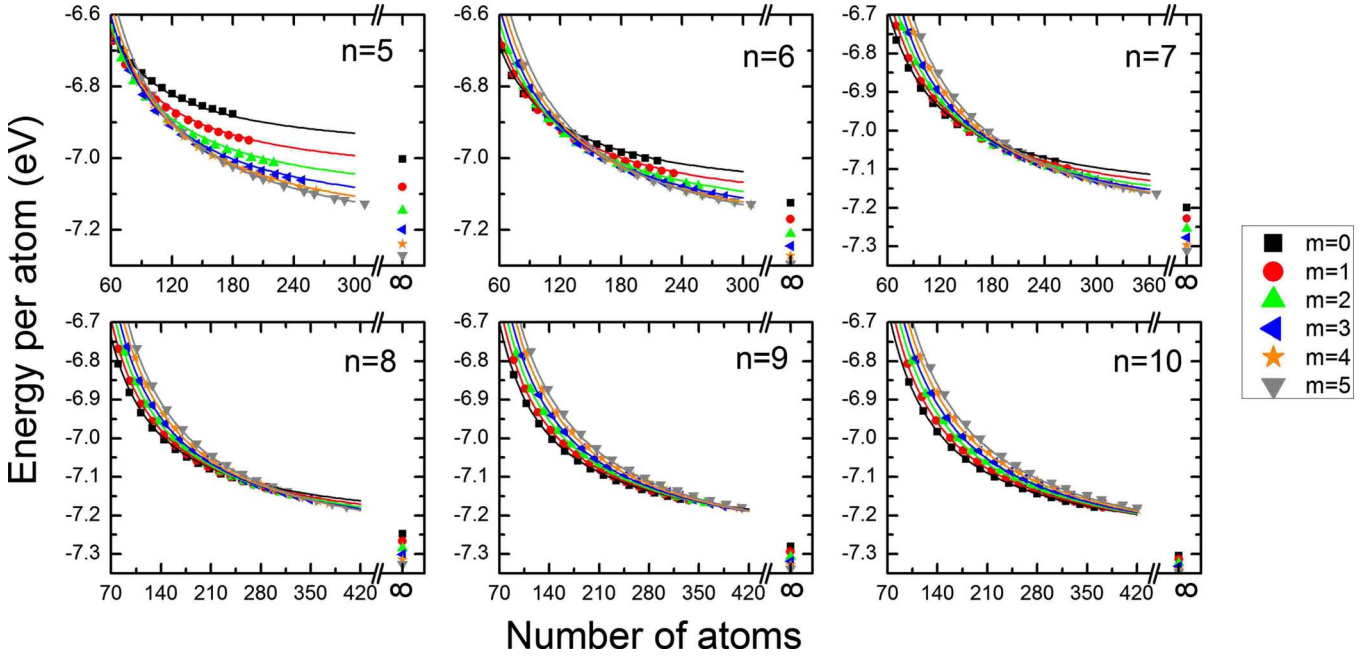

FIG. 4. (Color online) Comparison of the binding energy per atom calculated using the Tersoff potential and that obtained from the liquid surface model for the open end nanotubes. The curves show the values predicted by the model and different symbols (squares, triangles, stars, dots) correspond to the calculated values. The plots are shown for $n=5-10$. Each curve in one plot corresponds to a different m value.

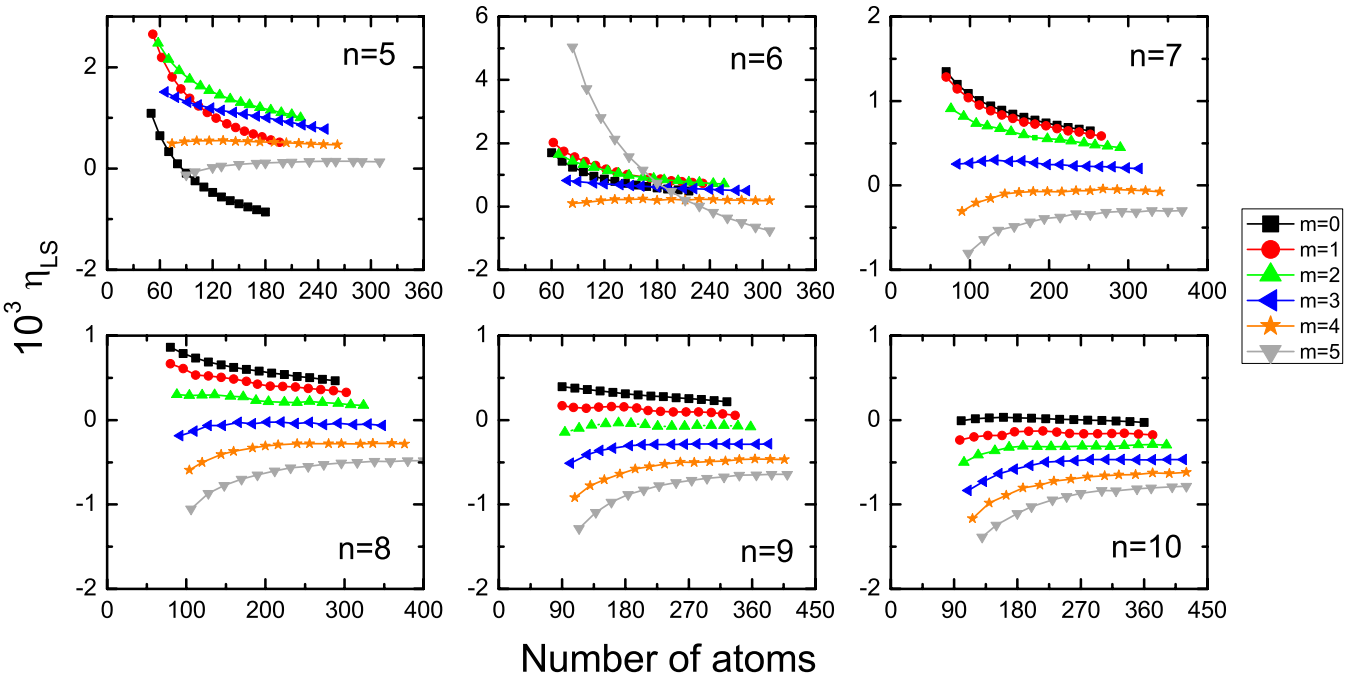

FIG. 5. (Color online) Relative deviation of the liquid surface model predictions of the binding energy per atom from that calculated using the Tersoff potential, Eq. (36), for the open end nanotubes. Plots are shown for $n=5-10$. Each curve in one plot corresponds to different m values.

$$\zeta = \frac{2\pi R}{L}. \tag{35}$$

If $\zeta \simeq 1$, the edge has a major influence on the nanotube energetics because in this case the size of the edge becomes comparable with the size of the inner part of the nanotube. As the nanotube grows in length, the parameter ζ, Eq. (35), decreases and in the limiting case (infinitely long nanotube) it reaches zero, reflecting the fact that the influence of the edge diminishes. The limiting values of the binding energy per atom for infinitely long nanotubes of different chirality are indicated in Fig. 4.

Another important feature shown in Fig. 4 is that the energetically favorable chirality of a nanotube depends on the total number of carbon atoms in it. As the total number of atoms increases, nanotubes with larger chiralities (higher radii) become energetically more favorable, whereas nanotubes of smaller radii are energetically favorable at smaller lengths. See, for example, top middle plot in Fig. 4, where this fact is clearly seen for nanotubes with $n=6$. When the total number of atoms in this example is less than 100, the binding energy per atom decreases with increase of m, while an opposite behavior is observed when the total number of atoms in the nanotube exceeds 180. This fact has a simple explanation. Figure 4 shows the dependence of the binding energy on the total number of atoms in the system. Thus, for a given number of atoms the length of a nanotube decreases if the radius of a nanotube grows. Therefore, nanotubes with smaller number of atoms (e.g., less than 100 for the $n=6$ case) with smaller value of the chirality number m are energetically more favorable, because the edge to length ratio ζ, Eq. (35), is smaller than in the case of nanotubes with larger m value.

If $L \gg R$, then the edge of a nanotube has a minor influence on its energetics. Therefore, nanotubes of larger radius should become energetically more favorable, since the curvature energy in this case is smaller.

In order to conclude about the accuracy of the liquid surface model, we determined the relative deviation of the binding energy per atom predicted by the liquid surface model from the binding energy per atom calculated using the Tersoff potential, which is defined as follows:

$$\eta_{LS} = \frac{\epsilon - \epsilon_{LS}}{\epsilon_{LS}}, \tag{36}$$

where ϵ_{LS} and ϵ are the binding energy per atom obtained from the liquid surface model and from calculations using the Tersoff potential respectively.

Figure 5 shows the relative deviation, η_{LS}, for nanotubes of different chiralities. In each plot, different curves correspond to different m values. The maximum relative deviation is found to be $\sim 0.2\%$. This illustrates that the liquid surface model is successful and can be used for predicting the energy of nanotubes.

The discussed model neglects the van der Waals energy between the atoms of a nanotube. In order to understand how the van der Waals interaction affects the energetics of the nanotubes, we have calculated the van der Waals energy per atom for nanotubes with $n=5$ to $n=10$ for arbitrarily selected m values. These calculations are performed with the MBN-Explorer package [68] and the parameters of the van der Waals interaction are taken from Ref. [69]. The van der Waals interaction between carbon atoms was parametrized with the Lennard-Jones potential with the equilibrium distance equal to 3 Å and the minimum energy 0.52 meV, as

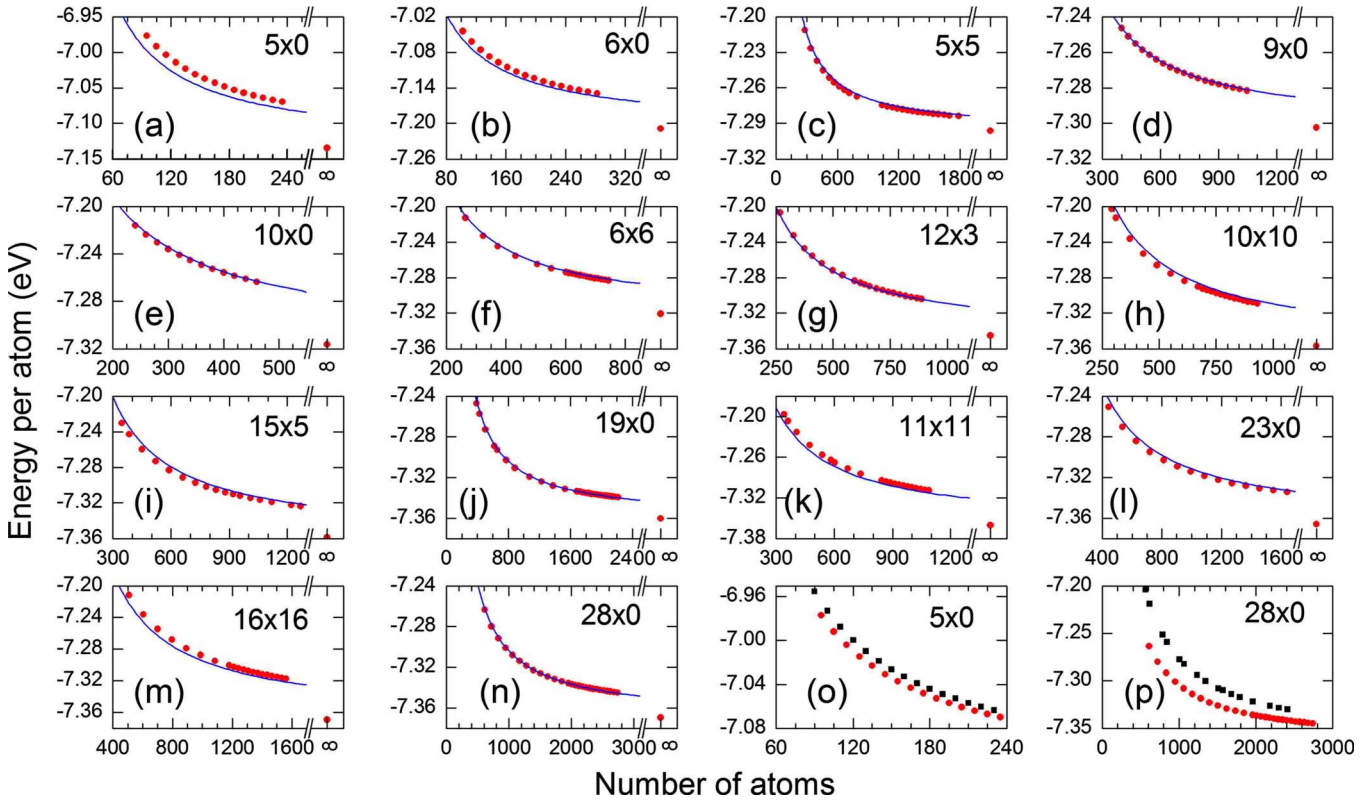

FIG. 6. (Color online) Plots (a)–(n): Comparison of the binding energy per atom calculated using the Brenner potential and that obtained from the liquid surface model for the capped nanotubes. The curves show the values predicted by the model and dots correspond to the calculated values. Plots (o) and (p) show the binding energies per atom calculated for capped (dots) and open end (squares) nanotubes of close sizes with chiralities (28,0) and (5,0). The chirality of the nanotubes is indicated in the inset to the plots.

suggested in Ref. [69] for fullerenes. The van der Waals interaction was calculated between all non-neighboring atoms, which were defined as atoms being more than 1.6 Å away from each other.

It has been observed that the van der Waals energy per atom is ~17–43 meV for all nanotubes, while the binding energy per atom is ~6.6–7.2 eV. Therefore, the van der Waals energy in nanotubes is almost negligible and we neglect it in our model.

Figure 6 shows the dependence of the binding energy per atom on the nanotube size calculated for the capped nanotubes with the use of the Brenner potential. Figure 7 illustrates the relative deviation of the binding energy per atom predicted by the liquid surface model from the corresponding values calculated with the use of the Brenner potential.

Figure 6 shows that the binding energy per atom for the capped nanotubes decreases with the increase of the nanotube length demonstrating the fact that longer nanotubes are energetically more favorable than the shorter ones. The relative deviation η_{LS}, Eq. (36), for the capped nanotubes, shown in Fig. 7 is below 0.3%, corresponding to the absolute energy difference of less then 0.01 eV ≈ 116 K. This energy difference is much below the energy of thermal vibrations in the system because the typical nanotube growth temperature is about 700–1200 K (see, e.g., Refs. [33,70,71]).

From Fig. 7 it can be noted that the relative deviation of energy is larger for shorter nanotubes. This happens because we neglect the cap deviation from a semisphere, as discussed in the preceding section. Indeed for shorter nanotubes the cap has a stronger impact on the binding energy per atom and therefore accounting for its deformation in this case becomes more important.

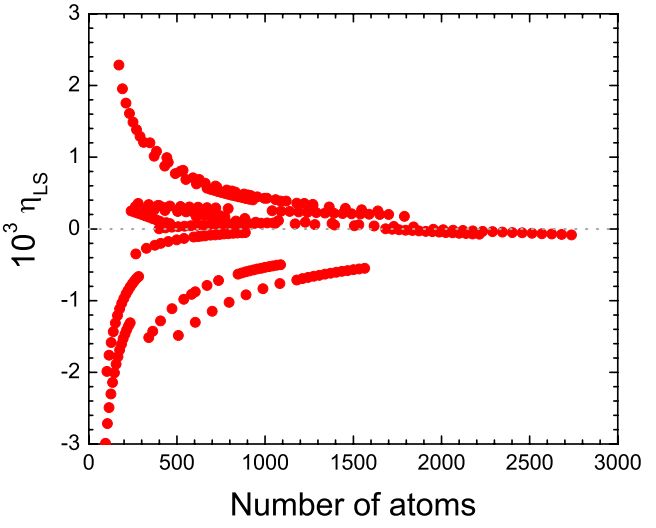

FIG. 7. (Color online) Relative deviation of the liquid surface model predictions of the binding energy per atom from that calculated using the Brenner potential, Eq. (36), for the capped nanotubes. Each dot in the plot corresponds to a certain nanotube of a given length and chirality.

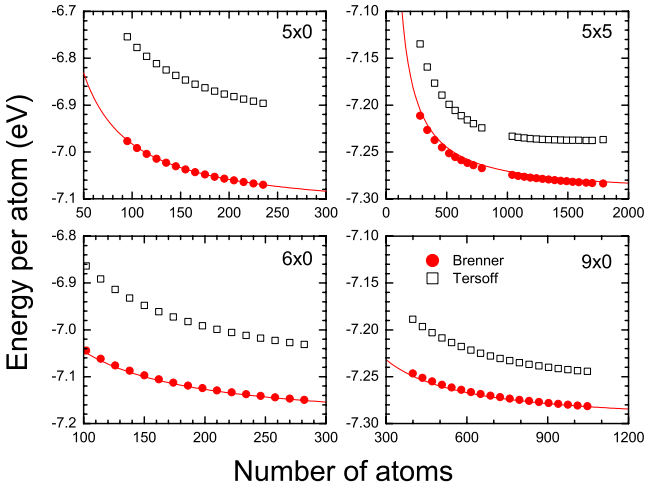

FIG. 8. (Color online) Comparison of the binding energy per atom calculated using Brenner (dots) and Tersoff (squares) potentials for capped nanotubes with chirality (5,0); (5,5); (6,0); (9,0). The line shows the binding energy per atom calculated using the liquid surface model.

In the last two plots in Fig. 6 we compare the binding energies per atom calculated for the capped and open end nanotubes of close sizes with chiralities (28,0) and (5,0). The comparison shows that the binding energy per atom for the open end nanotubes is higher than the binding energy per atom for the capped nanotubes because open end nanotubes have more dangling bonds at the edge and therefore are energetically less favorable. The differences in energies of open end and capped nanotubes arise only for nanotubes of finite length where the edge atoms play an important role, while for infinitely long structures the binding energies per atom are identical. This behavior is seen in Fig. 6, where the difference between the binding energy per atom for the open end and capped nanotubes is higher for shorter nanotubes than for the longer ones.

C. Comparison of Tersoff and Brenner potentials

It is believed that Brenner potential accounts more accurately for the π-bondings in the system, and therefore is better for the description of carbon nanotubes [11,59,60]. To stress the differences between the Tersoff and the Brenner potential in Fig. 8 we compare the binding energy per atom calculated with the use of both methods for capped nanotubes of several chiralities. Figure 8 shows that the binding energy per atom calculated with the use of Tersoff potential is higher than the binding energy per atom calculated with the use of Brenner potential. The energy difference is decreasing with the radius of the nanotube and is approximately equal to 0.13 eV, 0.08 eV, 0.03 eV, and 0.02 eV for nanotubes with chiralities (5,0), (6,0), (5,5), and (9,0), respectively, being less than 1% of the absolute value of the binding energy per atom in the nanotube.

The comparison in Fig. 8 demonstrates that the difference between the energies calculated with the use of Brenner and Tersoff potentials decrease with the nanotube radius leading to a conclusion that for nanotubes of higher radii [i.e., with chirality (19,0) or (28,0)] it should be almost negligible and both potentials become equivalent. However on the basis of the calculated differences of the binding energies it is impossible to judge which potential describes nanotubes more accurately because the asymptotic of the potentials depends on the form of the parametrization. In order to make the judgement on the quality of Brenner and Tersoff potentials we have used the calculated energies to determine the curvature constant and the Young modulus for single-wall carbon nanotubes and compared the obtained values with available experimental data and results of earlier calculations.

To relate the calculated energies to elastic properties of nanotubes let us consider a graphene sheet which we bend to form a nanotube of radius R. Within the framework of a continuum elastic model the curvature energy of the sheet can be written as follows [17,21,72–74]:

$$E_c = \frac{\pi E L d^3}{12R}, \tag{37}$$

where E is the Young modulus of the graphene sheet, d is its thickness, and L is the length of the nanotube. The length of the nanotube can be expressed via the total number of atoms N as follows:

$$L = \frac{S_i}{2\pi R} = \frac{\rho_i (N - N_e - N_{\text{cap}})}{2\pi R}, \tag{38}$$

where S_i is the surface area of the tubular part of the nanotube, N_e is the number of atoms at the edge, and N_{cap} is the number of atoms in the cap (see Fig. 2). Substituting Eq. (38) into Eq. (37) one obtains

$$E_c = \frac{E d^3 \rho_i}{24R^2} N - \frac{E d^3 \rho_i}{24R^2} N_e - \frac{\pi E d^3 \rho_i}{12 \rho_{\text{cap}}}. \tag{39}$$

The first term in Eq. (39) corresponds to the curvature energy of the tubular part of the nanotube which is equal to the second term in the large parentheses in Eq. (22). Thus,

$$\frac{C}{R^2} = \frac{E d^3 \rho_i}{24R^2} = \frac{\sqrt{3}\pi^2 \epsilon_c}{n^2 + m^2 + nm}. \tag{40}$$

Here C is the curvature constant,

$$C = \frac{3\sqrt{3}\langle a \rangle^2}{4} \epsilon_c \equiv \rho_i \epsilon_c. \tag{41}$$

Substituting the curvature constant, Eq. (41) into Eq. (40) one obtains

$$E = \frac{24 \epsilon_c}{d^3}. \tag{42}$$

The curvature constant C has been a subject of many investigations [17,18,21,22,57,73,75–78]. With $\langle a \rangle = 1.41$ Å and Eq. (41) one obtains $C_{\text{ters}} = 1.5183$ eV Å^2 for the Tersoff potential calculations and $C_{\text{bren}} = 0.9168$ eV Å^2 for the Brenner potential calculations. C_{ters} is very close to the value 1.57 eV Å^2 extracted from the measured phonon spectrum of graphite [77] and is in agreement with 1.44 eV Å^2, 1.34 eV Å^2, and 1.53 eV Å^2, which were calculated in Refs. [18,57,78]. These values were calculated with the use of em-

pirical potentials and using the tight-binding model. *Ab initio* density functional theory calculations lead to a somewhat higher value of the curvature constant. Thus the values 2.0 eV Å^2, 2.9 eV Å^2, and 2.14 eV Å^2 were reported in Refs. [22,73,75].

The curvature constants reported earlier are in better agreement with the result obtained for the open end nanotubes using the Tersoff potential than with the value C_{bren} calculated using Brenner potential. This fact shows that the Tersoff potential describes elastic properties of the nanotubes more accurately.

Young modulus is another important characteristic of the nanotubes. Researchers have reported widely varying Young's modulus values for carbon nanotubes in the range 0.32–5.5 TPa [15,16,18–23,77]. The large scatter of these values is apparently due to different measurement techniques, simulation methods, and dimensions (diameter, thickness, and configuration). As seen from Eq. (42) the Young modulus depends on the effective thickness of the graphene layer d. In Ref. [16] and Ref. [18] it has been suggested that the thickness of a graphene sheet is equal to 0.66 Å and 0.74 Å, respectively, being the radius of a single carbon atom. In Refs. [17,19] the thickness 3.4 Å was used, which is equal to the interplane distance in graphite. For our estimates we use $d=1.5$ Å which is approximately equal to the intercarbon distance in graphene. This value corresponds to the thickness of a fullerene shell [79] as reported by Rüdel *et al.* [80]. Thus we obtain $E_{\text{ters}}=0.670$ TPa and $E_{\text{bren}}=0.404$ TPa. Both values are within the ranges reported earlier indicating that the Tersoff and the Brenner potentials adequately describe the elastic properties of the nanotubes.

Despite the differences in results obtained using the Brenner and the Tersoff potentials, the liquid surface model is a universal tool. Differences between the potentials can always be accounted for by the parameters without changing the general framework of the model. Thus, it is feasible to derive the liquid surface model parameters from the comparison of its predictions with the results of *ab initio* calculations being based on LDA approximation or the Hartree-Fock theory.

D. Accounting for catalytic nanoparticle

It is experimentally known that when capped nanotubes grow from a catalytic nanoparticle [33,35,53], they have no open edges. The noncapped edge of a nanotube is embedded in the catalytic particle, which changes the interaction energy of the atoms in the vicinity of the contact.

In order to understand how the interaction of a nanotube with the catalytic nanoparticle influence the stability of a nanotube we use the model developed in Ref. [42] for calculating the interaction of a deposited cluster with a substrate. The catalytic nanoparticle is typically composed of Ni, Co or Fe atoms and the carbon atoms from feedstock molecules diffuse inside from the catalytic region towards the growth region [32–34]. Thus, in the following discussion we consider the catalytic nanoparticle being composed of a mixture of nickel and carbon atoms, as schematically illustrated in Fig. 9. The atoms of the catalytic nanoparticle interact with the carbon atoms of the nanotube via the Morse potential,

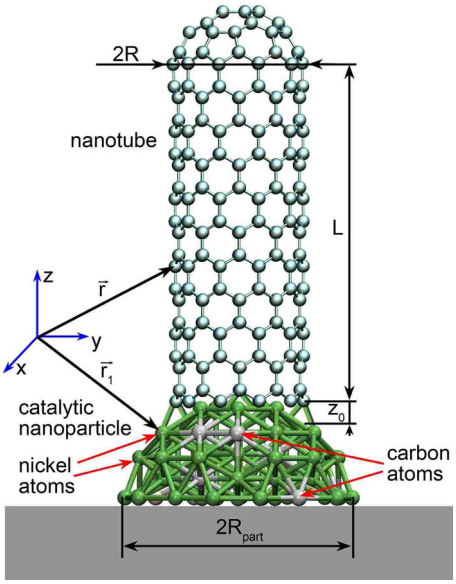

FIG. 9. (Color online) Single-wall carbon nanotube atop a catalytic nickel nanoparticle, z_0 is the distance between the nanotube and the catalytic nanoparticle, L is the length of the nanotube, R is the nanotube radius, and R_{part} is the radius of the nanoparticle.

$$U_k(r) = \varepsilon_k(\{1 - \exp[-\rho_k(r - r_{0_k})]\}^2 - 1). \tag{43}$$

Here r is the distance between an atom of the nanotube and an atom of the catalytic particle, ε_k, ρ_k, and r_{0_k} are parameters of the potential. Index k denotes either carbon-carbon (C) or carbon-nickel (Ni) interaction.

The Morse parameters ρ and r_0 are 2.625 Å^{-1} and 1.39 Å for the C-C interaction [81], while for the C-Ni interaction these parameters are 1.9213 Å^{-1} and 1.7518 Å, respectively [82]. The parameter ε is varied in different papers by more than an order of magnitude. For example in Ref. [82] it is 2.4781 eV for the C-Ni interaction, while in Ref. [83] it is 0.1 eV. The parameter ε for the C-C interaction is usually taken as 3.7–3.8 eV [81,84].

With the use of formalism developed in Ref. [42] the interaction energy of a nanotube with the catalytic nanoparticle can be estimated as

$$E_{\text{int}} = \frac{2\pi R n_{\text{C}}}{S_0} \int_{V_n} \int_{z_0}^{L+z_0} U_{\text{C}}(|\mathbf{r} - \mathbf{r}_1|) dV_1 dz + \frac{2\pi R n_{\text{Ni}}}{S_0} \int_{V_n} \int_{z_0}^{L+z_0} U_{\text{Ni}}(|\mathbf{r} - \mathbf{r}_1|) dV_1 dz, \tag{44}$$

where $n_{\text{C}}=N_{\text{C}}/V_n$ and $n_{\text{Ni}}=N_{\text{Ni}}/V_n$ are the concentrations of carbon and nickel in the catalytic nanoparticle, V_n is the volume of the nanoparticle, S_0 is the cross-section area of a single carbon atom, and z_0 is the distance between the catalytic particle and the nanotube (see Fig. 9). $\mathbf{r}=\mathbf{i}x+\mathbf{j}y+\mathbf{k}z$ is the vector describing an atom in the nanotube ($\mathbf{i}$, $\mathbf{j}$, and $\mathbf{k}$ are the unit basis vectors), while $\mathbf{r_1}$ is the vector which describes an atom in the catalytic nanoparticle (see Fig. 9). Equation (44) can be written as follows:

$$E_{\text{int}} = -\varepsilon_C \cdot N_C \cdot \alpha_C(z_0, R_{\text{part}}, R) - \varepsilon_{\text{Ni}} \cdot N_{\text{Ni}} \cdot \alpha_{\text{Ni}}(z_0, R_{\text{part}}, R), \tag{45}$$

where $\alpha_C, \alpha_{\text{Ni}}$ are dimensionless functions defining interactions determined by the size and topology of the catalytic nanoparticle defined by the integrals in Eq. (44) as follows:

$$\alpha_k = \frac{2\pi R}{V_n S_0} \int_{V_n} \int_{z_0}^{L+z_0} [(1 - e^{-\rho_k(|\mathbf{r}-\mathbf{r}_1|-r_{0_k})})^2 - 1] dV_1 dz. \tag{46}$$

Let us consider the binding energy per atom for a nanotube of chirality (28,0) accounting for the interaction with catalytic nanoparticle. According to Eq. (19) the radius of this nanotube is equal to $R_{28\times0}=10.88$ Å. We assume the catalytic nanoparticle to be a sphere of radius $R_{\text{part}}=2R_{28\times0}$ (see Fig. 9), thus the total number of atoms in the catalytic nanoparticle can be estimated as $N_{\text{total}} \approx V_n / V_{\text{Ni}}$, where $V_{\text{Ni}} = 4/3\pi R_{\text{Ni}}^3$ is the effective volume of a single nickel atom. With $R_{\text{Ni}} \approx 1.245$ Å one obtains $N_{\text{total}} \approx 5340$.

Let us assume the fraction of carbon atoms in the catalytic nanoparticle to be 0.1, resulting in $N_C=534$ and $N_{\text{Ni}}=4806$. The distance between the nanotube and the nanoparticle, $z_0 \approx 0.9$ Å, being the distance at which the interaction energy of a single carbon atom with an infinite crystal of nickel atoms has a minimum. Substituting the numbers into Eq. (46) and calculating S_0 from Eq. (20) one obtains $\alpha_C = 0.0033$, and $\alpha_{\text{Ni}}=0.0122$. Substituting α_C, α_{Ni}, N_C, and N_{Ni} into Eq. (45) [$S_0 \equiv \rho_i$, defined in Eq. (45)] one obtains the correction to the total energy of a nanotube as a function of potential well depth for the C-C and C-Ni interactions ε_C and ε_{Ni}. Since the parameters ε_C and ε_{Ni} vary in different papers significantly we assume $\varepsilon_C = \varepsilon_{\text{Ni}} = \varepsilon$. We have varied ε in order to illustrate the influence of the catalytic nanoparticle on the nanotube stability.

In Fig. 10 we show the binding energy per atom calculated using the Brenner potential for the capped nanotube of chirality (28.0). Different lines show the binding energy per atom calculated using the liquid surface model with accounting for the interaction with the catalytic nanoparticle and correspond to the different values of parameter ε. The corresponding values of ε are given in the inset. From Fig. 10 it is clear that the catalytic nanoparticle changes the energetics of the nanotube dramatically. If the interaction of a nanotube with the catalytic nanoparticle is weak (i.e., the well depth of the interatomic potential is $\lesssim 1$ eV) than longer nanotubes are energetically more favorable, because the binding energy per atom decreases and the following condition is fulfilled:

$$E_{N+1} - E_N - E_1 < 0. \tag{47}$$

Here E_{N+1} and E_N are the energies of nanotubes with $N+1$ and N atoms, respectively, while $E_1=0$ is the energy of a single atom. If the condition Eq. (47) holds then attachment of additional atoms to the nanotube is energetically favorable resulting in its growth. Figure 10 shows that if the catalytic nanoparticle-nanotube interaction is strong (see curves calculated with $\varepsilon=1.2$ eV and $\varepsilon=1.5$ eV in Fig. 10) than the trend of the binding energy per atom changes and it becomes energetically more favorable for the nanotube to collapse.

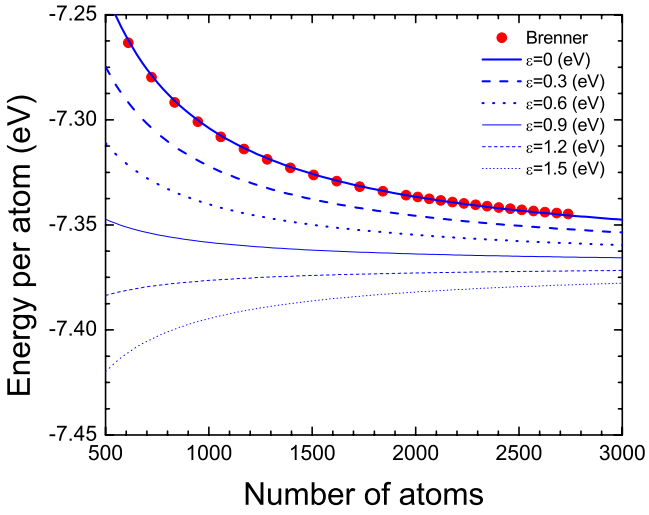

FIG. 10. (Color online) Binding energy per atom calculated using the Brenner potential (dots) for a capped nanotube of chirality (28,0). Different lines show the binding energy per atom calculated using the liquid surface model with accounting for the interaction with the catalytic nanoparticle and correspond to the different values of the parameter ε which describes the interatomic interaction. The corresponding values of ε are indicated in the inset.

IV. CONCLUSIONS

Many of the important properties of nanotubes depend on their energetics. We have developed a model which is capable to predict the energies of single-wall nanotubes with high accuracy once the chirality and the total number of atoms are known. Even with empirical potentials, like Tersoff potential, there are limitations on the size of nanotubes whose energy can be calculated. Hence, the developed liquid surface model serves as a potential candidate for the energy calculation of very large nanotubes.

The liquid surface model was suggested for open end and capped nanotubes. It was shown that the energy of capped nanotubes is determined by five physical parameters, while for the open end nanotubes three parameters are sufficient. The parameters of the liquid surface model were determined from the calculations performed with the use of empirical Tersoff and Brenner potentials and the accuracy of the model was analyzed. It was shown that the liquid surface model can predict the binding energy per atom for nanotubes with relative error below 0.3%, corresponding to the absolute energy difference being less then 0.01 eV.

The influence of the catalytic nanoparticle, atop which nanotubes grow, on the nanotube energetics was also discussed. It was demonstrated that the catalytic nanoparticle changes the binding energy per atom dramatically. In particular, it was shown that if the interaction of a nanotube with the catalytic nanoparticle is weak (i.e., $\lesssim 1$ eV) than attachment of an additional atom to a nanotube is an energetically favorable process, while if the catalytic nanoparticle-nanotube interaction is strong ($\gtrsim 1$ eV), it becomes energetically more favorable for the nanotube to collapse. The suggested model gives an important insight in the energetics and stability of nanotubes of different chirality and is an impor-

tant step towards the understanding of nanotube growth process.

We have also analyzed elastic properties of nanotubes and have performed a comparison with available experimental measurements and earlier theoretical predictions. Namely, we have calculated the Young modulus and the curvature constant for single-wall carbon nanotubes from the parameters of the liquid surface model and demonstrated that the obtained values are in agreement with the values reported earlier. The calculated Young modulus and the curvature constant were used to conclude about the accuracy of the Tersoff and the Brenner potentials. The elastic properties were derived from the parameters of the liquid surface model obtained from the Tersoff and the Brenner potential calculations and therefore correspond to the values calculated within the framework of the Tersoff and the Brenner potential, respectively. It was shown that the obtained values of the Young modulus and the curvature constant are within the ranges of values reported earlier for both potentials indicating that the Tersoff and the Brenner potentials adequately describe the elastic properties of nanotubes.

The liquid surface model has many potential applications. By including additional energy terms it can be used for the study of energetics and mechanical properties of deformed nanotubes such as toroidal and helical. Such nanotubes are getting wider attention nowadays because of the observation that one can change the electrical properties of nanotubes by deforming them. Another important property which can be studied using liquid surface model is the energetics of interacting nanotubes, such as, for example, nanotubes in a crystalline array. Adding a volume energy term corresponding to the interaction between different walls would allow the liquid surface model to be used for the study of the energetics of multiwall carbon nanotubes, which is left open for future considerations and analysis.

ACKNOWLEDGMENTS

The possibility to perform complex computer simulations at the Frankfurt Center for Scientific Computing is gratefully acknowledged. This work is partially supported by the European Commission within the Network of Excellence project EXCELL. We are very grateful to Ying Yin (University of Illinois at Urbana Champaign) for providing us with the code for nanotube geometry generation, which helped us to generate structures of nanotubes of different chiralities prior to their optimization.

[1] S. Iijima, Nature (London) **354**, 56 (1991).
[2] J. Bernholc, D. Brenner, M. Buongiorno Nardelli, V. Meunier, and C. Roland, Annu. Rev. Mater. Res. **32**, 347 (2002).
[3] R. S. Ruoff, D. Qian, and W. K. Liu, C. R. Phys. **4**, 993 (2003).
[4] Y. Akai and S. Saito, Physica E (Amsterdam) **29**, 555 (2005).
[5] M. Dresselhaus, G. Dresselhaus, and A. Jorio, Annu. Rev. Mater. Res. **34**, 247 (2004).
[6] A. Rubio, Appl. Phys. A: Mater. Sci. Process. **68**, 275 (1999).
[7] R. Saito, G. Dresselhaus, and M. S. Dresselhaus, *Physical Properties of Carbon Nanotubes* (Imperial College Press, London, 1999).
[8] S. Huang, X. Cai, and J. Liu, J. Am. Chem. Soc. **125**, 5636 (2003).
[9] J. P. Lu, Phys. Rev. Lett. **79**, 1297 (1997).
[10] J. Cai, R. F. Bie, X. M. Tan, and C. Lu, Physica B **344**, 99 (2004).
[11] P. Zhang, Y. Huang, P. H. Geubelle, P. A. Klein, and K. C. Hwang, Int. J. Solids Struct. **39**, 3893 (2002).
[12] M. M. J. Treacy, T. W. Ebbensen, and J. M. Gibson, Nature (London) **381**, 678 (1996).
[13] T. W. Tombler, C. Zhou, L. Alexseyev, J. Kong, H. Dai, L. Liu, C. S. Jayanthi, M. Tang, and S.-Y. Wu, Nature (London) **405**, 769 (2000).
[14] V. N. Popov, V. E. Van Doren, and M. Balkanski, Phys. Rev. B **61**, 3078 (2000).
[15] C. Reddy, S. Rajendran, and K. M. Liew, Nanotechnology **17**, 864 (2006).
[16] L. Wang, Q. Zheng, J. Z. Liu, and Q. Jiang, Phys. Rev. Lett. **95**, 105501 (2005).
[17] D. H. Robertson, D. W. Brenner, and J. W. Mintmire, Phys. Rev. B **45**, 12592 (1992).
[18] Zhou Xin, Zhou Jianjun, and Ou-Yang Zhong-can, Phys. Rev. B **62**, 13692 (2000).
[19] G. Van Lier, C. Van Alsenoy, V. Van Doren, and P. Geerlings, Chem. Phys. Lett. **326**, 181 (2000).
[20] M.-F. Yu, B. S. Files, S. Arepalli, and R. S. Ruoff, Phys. Rev. Lett. **84**, 5552 (2000).
[21] S. Gupta, K. Dharamvir, and V. K. Jindal, Phys. Rev. B **72**, 165428 (2005).
[22] D. Sánchez-Portal, E. Artacho, J. M. Soler, A. Rubio, and P. Ordejón, Phys. Rev. B **59**, 12678 (1999).
[23] E. Hernández, C. Goze, P. Bernier, and A. Rubio, Phys. Rev. Lett. **80**, 4502 (1998).
[24] D. J. Celentano and J.-L. Chaboche, Int. J. Plast. **23**, 1739 (2007).
[25] C. F. Cornwell and L. T. Wille, Solid State Commun. **101**, 555 (1997).
[26] B. I. Yakobson, C. J. Brabec, and J. Bernholc, Phys. Rev. Lett. **76**, 2511 (1996).
[27] S. Karmakar, S. M. Sharma, P. V. Teredesai, and A. K. Sood, Phys. Rev. B **69**, 165414 (2004).
[28] M. J. Peters, L. E. McNeil, J. P. Lu, and D. Kalm, Phys. Rev. B **61**, 5939 (2000).
[29] S. Reich, C. Thomsen, and P. Ordejón, Phys. Status Solidi B **235**, 354 (2003).
[30] S. Iijima, C. Brabec, A. Maiti, and J. Bernholc, J. Chem. Phys. **104**, 2089 (1996).
[31] E. W. Wong, P. E. Sheehan, and C. M. Lieber, Science **277**, 1971 (1997).
[32] B. Zheng, C. Lu, G. Gu, A. Makarovski, G. Finkelstein, and J. Liu, Nano Lett. **2**, 895 (2002).

[33] J. Geng, C. Singh, D. S. Shephard, M. S. P. Shaffer, B. F. G. Johnson, and A. H. Windle, Chem. Commun. (Cambridge) **2002**, 2666.
[34] D. Dobkin and M. Zuraw, *Principles of Chemical Vapor Deposition* (Springer, New York, 2003).
[35] S. Hofmann, G. Csanyi, A. C. Ferrari, M. C. Payne, and J. Robertson, Phys. Rev. Lett. **95**, 036101 (2005).
[36] V. N. Popov, New J. Phys. **6**, 17 (2004).
[37] K. Tanaka, K. Okahara, M. Okada, and T. Yamabe, Chem. Phys. Lett. **191**, 469 (1992).
[38] C. Zhou, J. Kong, and H. Dai, Appl. Phys. Lett. **76**, 1597 (2000).
[39] N. Bohr and J. A. Wheeler, Phys. Rev. **56**, 426 (1939).
[40] I. A. Solov'yov, A. V. Solov'yov, and W. Greiner, Int. J. Mod. Phys. E **13**, 697 (2004).
[41] I. A. Solov'yov, A. V. Solov'yov, W. Greiner, A. Koshelev, and A. Shutovich, Phys. Rev. Lett. **90**, 053401 (2003).
[42] V. V. Semenikhina, A. Lyalin, A. V. Solov'yov, and W. Greiner, J. Exp. Theor. Phys. **106**, 678 (2008).
[43] D. Poenaru, R. Gherghescu, I. Plonski, A. Solov'yov, and W. Greiner, Eur. Phys. J. D **47**, 379 (2008).
[44] D. Poenaru, R. Georgescu, A. Solov'yov, and W. Greiner, Europhys. Lett. **79**, 63001 (2007).
[45] H. Jiang, P. Zhang, B. Liu, Y. Huang, P. H. Geubelle, H. Gao, and K. C. Hwang, Comput. Mater. Sci. **28**, 429 (2003).
[46] X. Sun and W. Zhao, Mater. Sci. Eng., A **390**, 366 (2005).
[47] K. Kanamitsu and S. Saito, J. Phys. Soc. Jpn. **71**, 483 (2002).
[48] M. J. López, I. Cabria, N. H. March, and J. A. Alonso, Carbon **43**, 1371 (2005).
[49] M. F. Budyka, T. S. Zyubina, A. G. Ryabenko, S. H. Lin, and A. M. Mebel, Chem. Phys. Lett. **407**, 266 (2005).
[50] Ş. Erkoç and S. Özkaymak, Eur. Phys. J. D **4**, 331 (1998).
[51] D. Tang, S. Xie, W. Liu, B. Chang, L. Sun, Z. Liu, G. Wan, and W. Zhou, Carbon **38**, 480 (2000).
[52] N. de Jonge, M. Doytcheva, M. Allioux, M. Kaiser, S. A. M. Mentink, K. B. Teo, R. G. Lacerda, and W. I. Milne, Adv. Mater. (Weinheim, Ger.) **17**, 451 (2005).
[53] O. A. Louchev, Y. Sato, and H. Kanda, Phys. Rev. E **66**, 011601 (2002).
[54] M. S. C. Mazzoni, H. Chacham, P. Ordejón, D. Sánchez-Portal, J. M. Soler, and E. Artacho, Phys. Rev. B **60**, R2208 (1999).
[55] R. Morjan, M. Kabir, S. Lee, O. Nerushev, P. Lundgren, S. Bengtsson, Y. Park, and E. Campbell, Curr. Appl. Phys. **4**, 591 (2004).
[56] A. V. Bazilevsky, K. Sun, A. L. Yarin, and C. M. Megaridis, J. Mater. Chem. **18**, 696 (2008).
[57] J. Tersoff, Phys. Rev. B **46**, 15546 (1992).
[58] J. Tersoff, Phys. Rev. B **37**, 6991 (1988).
[59] D. W. Brenner, Phys. Rev. B **42**, 9458 (1990).
[60] J. Che, T. Cagin, and W. A. Goddard III, Nanotechnology **10**, 263 (1999).
[61] M. S. Dresselhaus, G. Dresselhaus, and R. Saito, Carbon **33**, 883 (1995).
[62] J. Tersoff, Phys. Rev. Lett. **61**, 2879 (1988).
[63] H. Shen, Mater. Lett. **60**, 2050 (2006).
[64] R. T. Chancey, L. Oddershede, F. E. Harris, and J. R. Sabin, Phys. Rev. A **67**, 043203 (2003).
[65] P. A. Marcos, J. A. Alonso, A. Rubio, and M. J. López, Eur. Phys. J. D **6**, 221 (1999).
[66] M. J. López, A. Rubio, J. A. Alonso, L.-C. Qin, and S. Iijima, Phys. Rev. Lett. **86**, 3056 (2001).
[67] P. W. Fowler and D. E. Manolopoulos, *An Atlas of Fullerenes* (Dover, New York, 2007).
[68] I. Solov'yov, O. Obolensky, V. Semenikhina, A. Yakubovich, A. Lyalin, and A. Solovyov, Explorer 1.0.0, MBNS Group at FIAS, Frankfurt am Main, 2008.
[69] A. Hussien, A. Yakubovich, A. Solov'yov, and W. Greiner, e-print arXiv:0807.4435v1.
[70] S. Pal, S. Talapatra, S. Kar, L. Ci, R. Vajtai, T. Borca-Tasciuc, L. Schadler, and P. Ajayan, Nanotechnology **19**, 045610 (2008).
[71] C. J. Lee, J. Park, J. M. Kim, Y. Huh, J. Y. Lee, and K. S. No, Chem. Phys. Lett. **327**, 277 (2000).
[72] G. G. Tibbetts, J. Cryst. Growth **66**, 632 (1984).
[73] O. Gülseren, T. Yildirim, and S. Ciraci, Phys. Rev. B **65**, 153405 (2002).
[74] L. D. Landau, A. M. Kosevich, and E. M. Lifshitz, *Theory of Elasticity* (Butterworth, Heinemann, 1986).
[75] L. Li, S. Reich, and J. Robertson, J. Nanosci. Nanotechnol. **6**, 1290 (2006).
[76] K. N. Kudin, G. E. Scuseria, and B. I. Yakobson, Phys. Rev. B **64**, 235406 (2001).
[77] R. Nicklow, N. Wakabayashi, and H. Smith, Phys. Rev. B **5**, 4951 (1972).
[78] O.-Y. Zhong-can, Z.-B. Su, and C.-L. Wang, Phys. Rev. Lett. **78**, 4055 (1997).
[79] S. Lo, A. Korol, and A. Solov'yov, J. Phys. B **40**, 3973 (2007).
[80] A. Rüdel, R. Hentges, U. Becker, H. S. Chakraborty, M. E. Madjet, and J. M. Rost, Phys. Rev. Lett. **89**, 125503 (2002).
[81] T. Belytschko, S. P. Xiao, G. C. Schatz, and R. S. Ruoff, Phys. Rev. B **65**, 235430 (2002).
[82] Y. Shibuta and S. Maruyama, Comput. Mater. Sci. **39**, 842 (2007).
[83] Z.-C. Lin, J.-C. Huang, and Y.-R. Jeng, J. Mater. Process. Technol. **192-193**, 27 (2007).
[84] Y. Xiao, Z. M. Li, X. H. Yan, Y. Zhang, Y. L. Mao, and Y. R. Yang, Phys. Rev. B **71**, 233405 (2005).